Investigation into distinguishing between small volumetric and crack-like defects using multi-view total focusing method images

Jie Zhang, Tom Barber, Andrew Nixon, and Paul Wilcox

Citation: AIP Conference Proceedings **1806**, 040003 (2017); doi: 10.1063/1.4974590
View online: http://dx.doi.org/10.1063/1.4974590
View Table of Contents: http://aip.scitation.org/toc/apc/1806/1
Published by the American Institute of Physics

Investigation into Distinguishing between Small Volumetric and Crack-like Defects Using Multi-view Total Focusing Method Images

Jie Zhang[1, a)], Tom Barber[1, b)], Andrew Nixon[1, c)], and Paul Wilcox[1, d)]

[1]*Department of Mechanical Engineering, University Walk, University of Bristol, Bristol BS8 1TR, UK*

[a)]Corresponding author: j.zhang@bristol.ac.uk
[b)]t.s.barber@bristol.ac.uk, [c)]a.d.nixon@bristol.ac.uk and [d)]p.wilcox@bristol.ac.uk

Abstract. In the post-processing of ultrasonic array full matrix capture (FMC) data from an immersion inspection to image a region of interest (ROI), the total focusing method (TFM) can be used to generate multiple image views for the same region through exploiting reflections off geometric features, mode conversions at interfaces and using different paths for transmitted and received waves. They are termed as the multi-view TFM (MTFM) images. In this paper, the feasibility of using MTFM images to distinguish between small volumetric and crack-like defects is investigated through the analysis of the images from various simulated and experimentally-measured FMC array data sets. It is found that the presence of a defect of a particular type will typically be observable in some or all of the views with different image amplitudes. Different types of defect have large amplitudes in different views and this can be used to classify the defect type. Finally, the use of this approach is demonstrated in the experimental inspection of samples.

INTRODUCTION

A common problem in industrial NDT is the accurate characterization of defects identified in ultrasonic array images. A particular challenge is the distinction between volumetric defects (such as single gas pores and inclusions) and planar crack-like flaws. In recent years, the use of ultrasonic arrays for non-destructive evaluation (NDE) has been revolutionized by use of full matrix capture (FMC) [1] which records the time-domain signals associated with every possible transmitter-receiver element combination and allows images to be generated in post-processing using different imaging algorithms, such as the Total Focusing Method (TFM). For a FMC array data set captured using an immersion inspection configuration, TFM images showing multiple different views of the same region can be generated by exploiting reflections off geometric features, mode conversions at interfaces, and using different paths for transmitted and received waves. These images are termed as multi-view TFM (MTFM) images, with each view corresponding to a different path. Without any extra data capture, the analysis of these images can increase the performance of defect detection and characterization.

In this paper, the use of multi-view TFM images to distinguish between small volumetric and crack-like defects is investigated through the analysis of TFM images from various simulated and experimentally-measured FMC array data sets. The data is from samples containing various defects at the same position relative to the array. The defects have the same nominal size but different orientation angles and shapes. A hybrid forward model [2] is used to simulate the FMC array data sets for various modelled defects by simulating the propagation of signals along each possible path and superposing the results. An efficient method [3] combined with the Dijkstra ray-tracing method [4] is used

43rd Annual Review of Progress in Quantitative Nondestructive Evaluation, Volume 36
AIP Conf. Proc. 1806, 040003-1–040003-7; doi: 10.1063/1.4974590
Published by AIP Publishing. 978-0-7354-1474-7/$30.00

to calculate the focal laws for the paths associated with different views. Finally, the most suitable image views for distinguishing between volumetric and crack-like planar defects are chosen. Note that this paper is focused on distinguishing defects that have been detected, not on the detection itself.

HYBRID FORWARD MODEL

The hybrid forward model developed by the authors [2] is used to simulate the FMC array data sets for a number of modelled defects. This model combines scattering coefficient matrices [5] that model the wave–defect interactions with a ray-based model of wave propagation [6-7]. Reflections, transmissions [8] and mode conversions are also included by formulating the problem as an equivalent multi-layer wave propagation problem. In the frequency domain, the signal transmitted from an array element *i* and received by an element *j* for a defect at $\boldsymbol{q}$ can be expressed as,

$$G_{ij}(\boldsymbol{q},f) = \sum_{m=1}^{N_m} G_0(f) D_i(\boldsymbol{q},f,m) D_j(\boldsymbol{q},f,m) E_i(\boldsymbol{q},m) E_j(\boldsymbol{q},m) D_i(\boldsymbol{q},f,m) S_{ij}(\boldsymbol{q},f,m) \quad (1)$$

where *f* is the frequency, *m* is the index of a particular path from the *i*th transmitter element to a defect at $\boldsymbol{q}$ and back to the *j*th receiver element, G_0 is the frequency spectrum of the signal transmitted into the specimen, *D* is the directivity function of an array element [9], *E* is the transfer function of the layered system which includes transmission coefficient through the coupling interface, possible reflection coefficient from the back face of the specimen, the wave propagation function and the beam spread function [2], *S* is the far field S-matrix which is defined as the far-field complex amplitude of scattered signals from a scatterer as a function of the incident and scattering angles and frequency [5-6]. Note that there are analytical solutions available for calculating the S-matrices of various incident and scattered wave combination for circular holes and cracks [10-11]. The paths considered are listed in Table 1.

MULT-VIEW TOTAL FOCUSING METHOD

Mathematically, the intensity of the pixel at position, $\boldsymbol{r}$, in TFM image view m can be written as,

$$I_m(\boldsymbol{r}) = \left| \sum_i \sum_j g_{ij}\left(\tau_{ij}^{(m)}(\boldsymbol{r})\right) \right|, \quad (2)$$

where g_{ij} is the time domain signal transmitted from the ith element and received by the jth element and it is the inverse Fourier transform of equation (1), $\tau_{ij}^{(m)}(\boldsymbol{r})$ is the travelling time for a wave emitted from the element i to a pixel at $\boldsymbol{r}$ and back to the element j, along the mth path and is commonly referred to as a focal law. In this paper, an efficient method [3] combined with Dijkstra ray tracing method [4] is used to calculate the focal laws for each view.

Each view is described by two sequences of letters separated by a hyphen. Each letter corresponds to a leg of the path and is either L for longitudinal waves or T for shear waves. The sequence of letters before the hyphen denotes the path from the transmitting element to the image point (the transmission path) and the second sequence denotes the path from the image point back to the receiving element (the reception path). For an immersion inspection configuration, the first and last elements in a path are always L and correspond to longitudinal waves in water. Transmission and reception paths can be described as either direct if they do not involve a reflection off the back wall or half-skip if they do. At present, paths with further reflections are not considered and consequently a total path can be either direct, half-skip (i.e. either the transmission or the reception path is half-skip but not both) or full-skip (i.e. both transmission and reception paths are half-skip). Ignoring the water legs, the remaining letters in direct and half-skip transmission and reception paths come from one of the following 6 combinations: L, T, LL, LT, TL or TT. The total number of possible imaging modes is therefore a multi-subset problem and it is,

$$N_M = \left(\binom{n_c}{n_m} \right) = \frac{(n_c+n_m-1)!}{n_m!(n_c-1)!}, \quad (3)$$

where, n_c is the cardinality of the subset, n_m is the cardinality of the set from which the subsets are drawn. Here, n_c = 6 is the total number of possible transmission/reception paths, and

TABLE 1. Image view definition and its details.

view, (m)	path	Type
1	LL-LL	Direct
2	LL-TL	
3	LT-TL	
4	LLL-LL	Half Skip
5	LLL-TL	
6	LLT-LL	
7	LLT-TL	
8	LTL-LL	
9	LTL-TL	
10	LTT-LL	
11	LTT-TL	
12	LLL-LLL	Full Skip
13	LLL-LTL	
14	LLL-TLL	
15	LLL-TTL	
16	LLT-LTL	
17	LLT-TLL	
18	LLT-TTL	
19	LTL-LTL	
20	LTL-TTL	
21	LTT-TTL	

SIMULATION AND EXPERIMENTAL MEASUREMENT

Note that, in this paper, the investigation is concentrated on distinguishing volumetric defects (e.g. porosity) and planar defects (e.g. cracks) and is limited to the specific defects listed in Table 2. For simulation purposes, these scatterers are assumed to exist in a homogeneous isotropic specimen of thickness 5.5 mm and at a depth of 2.5 mm, i.e. at $(x,z) = (0, 2.5 \text{ mm})$. The amplitude of defect images are examined on 4 simulated and 4 experimentally measured defects. Note that electrical discharge machined (EDM) slots are used to simulate cracks in the physical sample. The specimen has a wave speeds v_2 = 5000 m/s and v_3 = 2500 m/s for longitudinal and shear waves respectively. The specification of the ultrasonic array used is listed in Table 3 and the inspection configuration is shown in Figure 1.

TABLE 2. Specification of simulated and experimentally measured defects

Defect label	Type	Size a, (mm)	Position (x,z) (mm)	Orientation angle α_d (°)
Defect 1	Side drilled circular hole	1	(0, 2.5)	
Defect 2	Lack of fusion crack/slot	1	(0, 2.5)	25
Defect 3	Vertical crack/slot	1	(0, 2.5)	0
Defect 4	Lack of fusion crack/slot	1	(0, 2.5)	-25

TABLE 3. Specification of the array probe used in simulation and experimental measurement

Number of element	Central frequency (MHz)	Element width (mm)	Element pitch (mm)
110	10	0.14	0.17

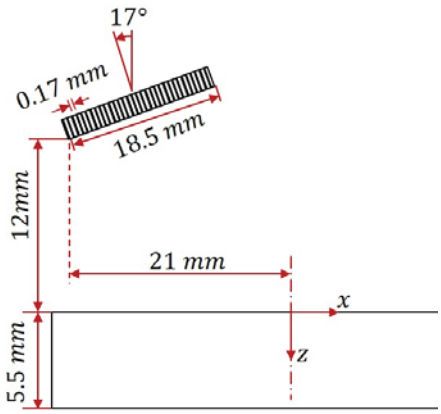

FIGURE 1. Schematic of array inspection configuration and defect positions used in simulation.

In the simulation and experimental measurements, for each FMC array data set, the TFM image for each of the views listed in Table 1 are generated. The peak amplitude at the defect location in each image is extracted and this is shown as a function of imaging view. Here the array configuration has stand-off h = 12 mm, inclination angle α = 17° and lateral offset l = 21 mm, is used in the simulation and experimental measurements to generate TFM images of the defects because they have to be detected in the first instance and then make characterisation.

Figure 2 compares the simulated and experimentally measured results from defects 1-4 listed in Table 2. Note that in this figure, image views which lead to large amplitudes for each defect have been chosen for comparison. The peak

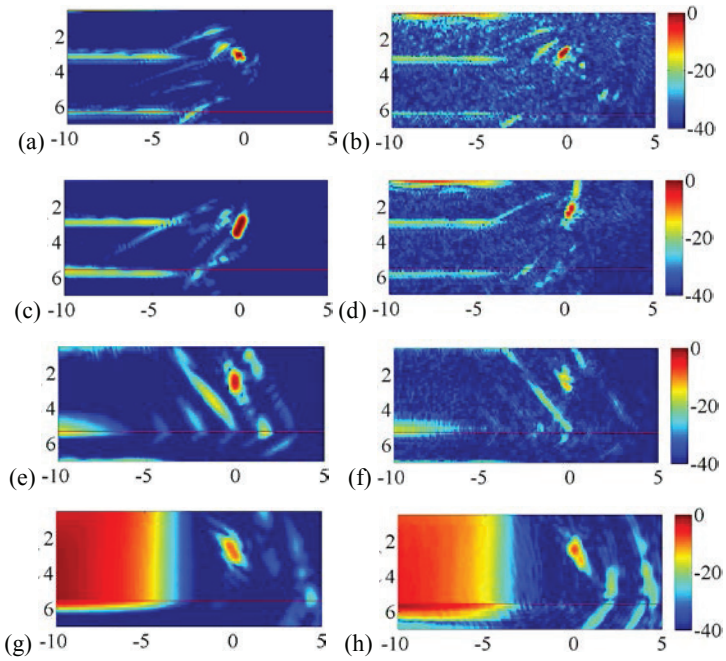

FIGURE 2. Comparison of the TFM images generated from: (a, c, e, g) the simulated FMC array data set and (b, d, f, h) the experimentally measured FMC array data set. (a,b) are the LT-TL views from defect 1 (SDH); (c,d) are the LT-TL views from defect 2 (crack at 25°); (e,f) are the LTT-TL views from defect 3 (vertical crack); (g,h) are the LLL-LL views from defect 4 (crack at -25°).

amplitude of the back wall image from the LL-LL image view is used as a reference to normalize all images from the same FMC data set. Generally speaking, the agreement between images from the simulated data set and the experimentally measured data set for each defect is good with respect to the location of the defect and any induced image artefacts. However, there are up to around 10 dB differences between the amplitudes from simulation and

experimental measurements. The best agreement between simulation and experimental measurement is shown in the images from defect 1 (1 mm diameter SDH). This is probably because in this case the shape of the modelled defect closely matches that of the physical defect. For the other defects, the geometric difference between modelled zero-width cracks and the round-ended, finite-width EDM slots used in the experiment is believed to be the main reason for the disagreement.

Figure 3 shows the LL-LL view for the four defects. As can be seen, the defect responses have different amplitudes in the different views and this is the basis of the method to distinguish them. For classification, statistically significant differences in measured defect amplitude as a function of image view are required.

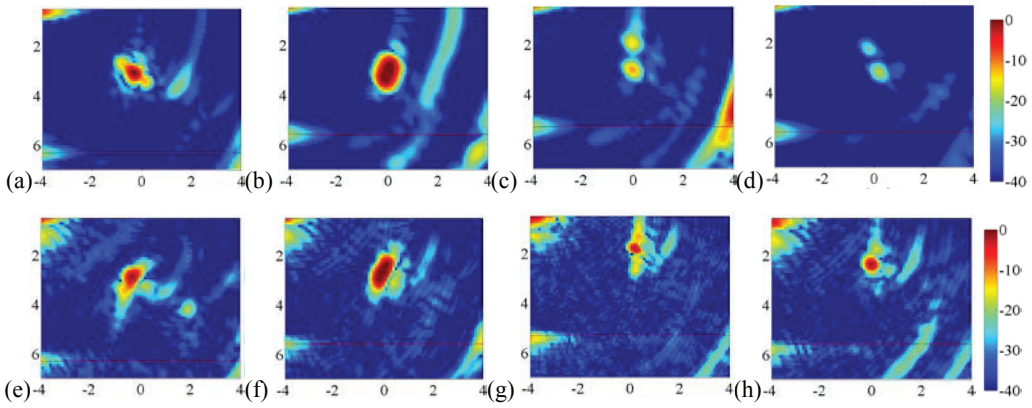

FIGURE 3. Comparison of LL-LL views from: (a-d) simulated data and (e-h) experimentally measured data. (a,e) are for defect 1 (SDH), (b,f) are for defect 2 (crack at 25°), (c, g) are for defect 3 (vertical crack) and (d,h) for defect 4 (crack at -25°).

It is found that, for the chosen specific defects, the large image amplitude difference can be seen from the views 1 (LL-LL), the views 2 (LL-TL), 19(LTL-LTL) and 21(LTT-TTL). Figures 4(a-d) show the image amplitude response at these chosen views from each crack/slot defect. The image views which lead to a large amplitude difference relative to the SDH are the candidate views for distinguishing the cracks/slots from the SDH. It is experimentally observed that the uncertainty in experimental measurements could cause variation of the measured amplitudes. Considering

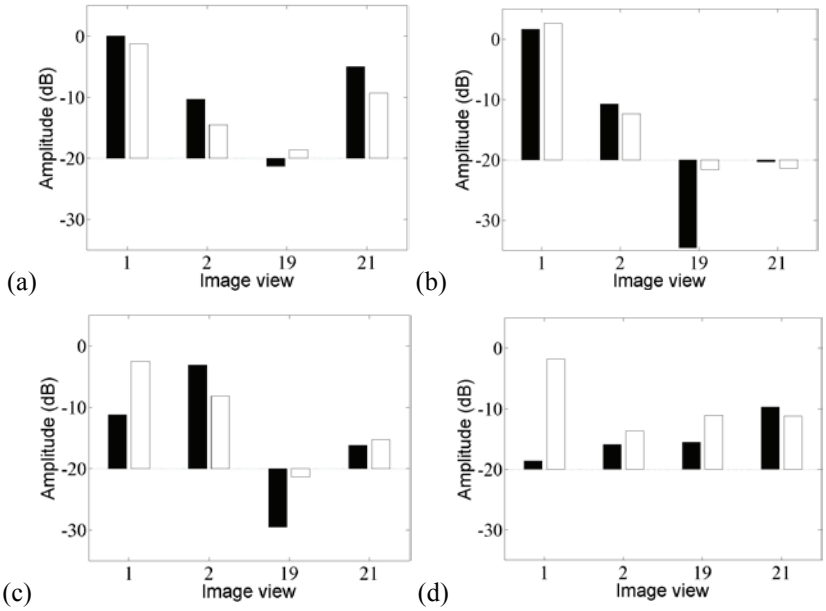

FIGURE 4. The comparison of the peak amplitude of defect images as a function of image view obtained from defect: (a-d) 1-4. Note that the black bars are from experimental measurements and the white bars from simulation.

there are around 3-5 dB measured variation in experimental measurements, only the imaging modes which lead to amplitude differences of over 5 dB between different defect types are assumed to provide potential for distinguishing defects.

The images from the chosen views to distinguish different defects are as demonstrated in Figures 5-6. In Figure 5, the LL-LL and LTT-TTL image views from a 1 mm diameter SDH and a 1 mm long crack/slot with an orientation angle of 25° are compared. As shown the images from the SDH have large amplitude in both image views while those from the crack have large amplitude difference. Also the image features from both defects are quite different.

In Figure 6, the LL-LL and LTL-LTL image views from a 1 mm long vertical crack/slot and a 1 mm long crack/slot with an orientation angle of 25° are compared. As shown the images from the 1 mm long crack/slot with an orientation angle of 25° have large amplitudes in both image views while those from another crack have large amplitude difference. Also the two crack tips can be seen the LL-LL image view from the vertical crack but not in the images from another crack.

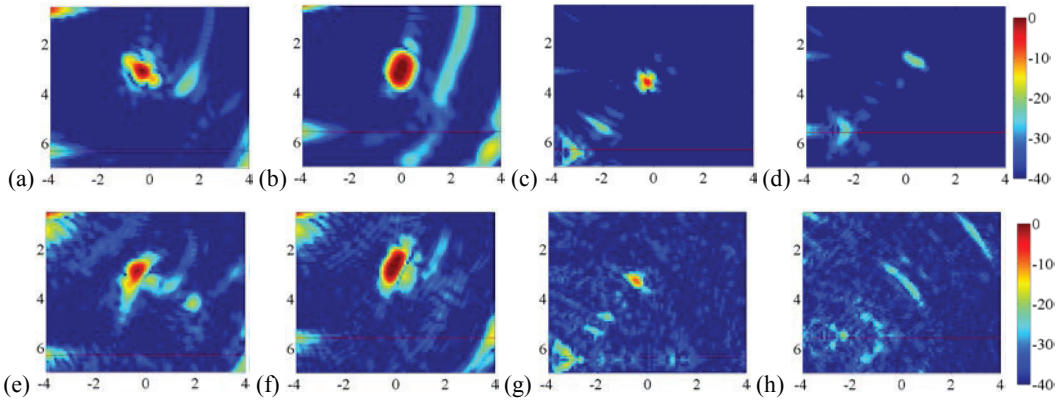

FIGURE 5. Comparison of the views from: (a-d) simulated data and (e-h) experimentally measured data. (a, c, e, g) are from defect 1 (SDH) and (b, d, f, h) are from defect 2 (crack at 25°). (a, b, e, f) are LL-LL views and (c, d, g, h) are LTT-TTL views.

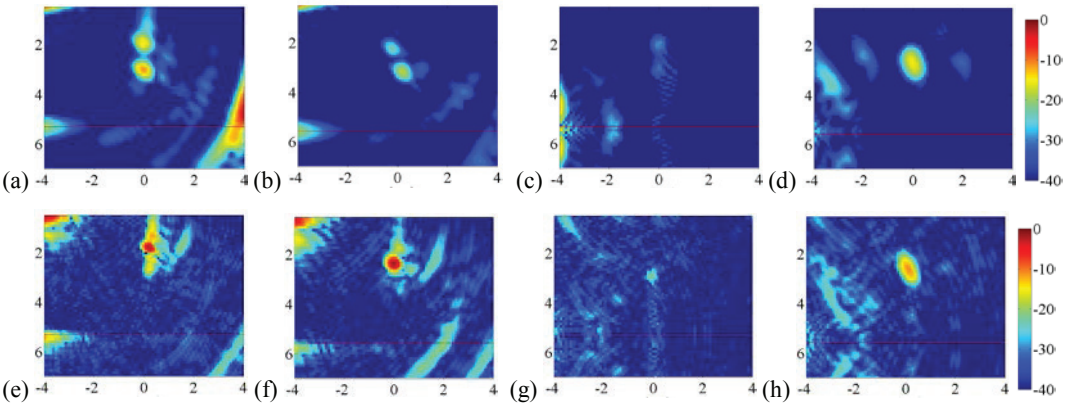

FIGURE 6. Comparison of the image views from: (a-d) simulated data and (e-h) experimentally measured data. (a, c, e, g) are from defect 3 (vertical crack/slot) and (b, d, f, h) are from defect 4 (crack/slot at -25°). (a, b, e, f) are from LL-LL views and (c, d, g, h) from LTL-LTL views.

In conclusion, the combination of image views can be used to distinguish the specific defects, for example: LL-LL and LTT-TTL image views can be used to distinguish the SDH and the 25° orientated crack/slot; LL-LL and LTL-LTL image views can be used to distinguish the vertical crack/slot and the -25° orientated crack/slot.

SUMMARY

The concept of MTFM based on FMC array data is proposed. A hybrid forward model is used to simulate FMC array data sets from an oblique immersion inspection. Through the MTFM images generated from both simulated and experimentally measured FMC data sets, it is shown that the presence of a defect of a particular type will typically be observable in some or all of the views with different image amplitudes. The differences in amplitude between views can be used to classify the defect type. It is demonstrated that it is feasible to distinguish volumetric and crack-like defects using MTFM images. Further experimental trials are required on more realistic crack-like defects.

ACKNOWLEDGMENTS

This work was supported by the Engineering and Physical Sciences Research Council through the Industrial Doctorate Centre in NDE(Grant no.GR/1411634/01). T Barber is also supported financially by the Royal Commission for the Exhibition of 1851.

REFERENCES

1. C. Holmes, B. W. Drinkwater and P. D. Wilcox, *NDT & E. Int.* 701-711, (2005).
2. J. Zhang, B. W. Drinkwater, P. D. Wilcox, and A. Hunter, *NDT & E. Int.* **43**, 123-133, (2010).
3. J. Zhang, B. Drinkwater, and P. Wilcox, *IEEE Trans. Ultrason. Ferr. Freq. Contr.* **61**, 1284-1295, (2014).
4. T. Moser, Geophysics, **56**, 59-67, (1991).
5. J. Zhang, B. Drinkwater, and P. Wilcox, *IEEE Trans. Ultrason. Ferr. Freq. Contr.* **55**, 2254-2265, (2008).
6. L. W. Schmerr, *Fundamentals of ultrasonic nondestructive evaluation - a modeling approach* (Plenum press, New York, 1998), pp. 305-371.
7. J. D. Achenbach, A. K. Gautesen and H. McMaken, *Ray methods for waves in elastic solids* (Pitman Advanced Publishing Program, Boston), pp. 1-9 (1992).
8. J. Krautkramer and H. Krautkramer, *Ultrasonic Testing of Materials* (New York: SpringerVerlag), pp. 563-567 (2003).
9. F. G. Miller and H. Pursey, *Proc. R. Soc. A-Math. Phys. Eng. Sci.*, **34**, 521-541 (1954).
10. A. L. Lopez-Sanchez, H. Kim, L. W. Schmerr Jr., and A. Sedov, *J. Nondestruct. Eval.* **24**, 83-96 (2005).
11. E. Glushkov, N. Gluskova, A. Ekhlakov and E. Shapar, *Wave Motion*, **43**, 458-473 (2006).